Journal of Alloys and Compounds 509 (2011) 4882–4886

Contents lists available at ScienceDirect

Journal of Alloys and Compounds

journal homepage: www.elsevier.com/locate/jallcom

Phase constituents and microstructure of laser cladding Al_2O_3/Ti_3Al reinforced ceramic layer on titanium alloy

Li Jianing[a], Chen Chuanzhong[a,*], Lin Zhaoqing[a], Tiziano Squartini[b]

[a] Key Laboratory for Liquid-Solid Structural Evolution and Processing of Materials (Ministry of Education), Department of Materials Science, Shandong University, Jing Shi Road # 17923, Jinan 250061, Shandong, China
[b] INFM – Department of Physics, Siena University, Siena 53100, Italy

ARTICLE INFO

Article history:
Received 7 January 2011
Received in revised form 23 January 2011
Accepted 27 January 2011
Available online 4 February 2011

Keywords:
Ceramics
Coating materials
Intermetallics
X-ray diffraction

ABSTRACT

Laser cladding of the $Fe_3Al + TiB_2/Al_2O_3$ pre-placed alloy powder on Ti–6Al–4V alloy can form the $Ti_3Al/Fe_3Al + TiB_2/Al_2O_3$ ceramic layer, which can greatly increase wear resistance of titanium alloy. In this study, the $Ti_3Al/Fe_3Al + TiB_2/Al_2O_3$ ceramic layer has been researched by means of electron probe, X-ray diffraction, scanning electron microscope and micro-analyzer. In cladding process, Al_2O_3 can react with TiB_2 leading to formation of amount of Ti_3Al and B. This principle can be used to improve the $Fe_3Al + TiB_2$ laser cladded coating, it was found that with addition of Al_2O_3, the microstructure performance and micro-hardness of the coating was obviously improved due to the action of the Al–Ti–B system and hard phases.

1. Introduction

Intermetallic compounds have been the subjects of intense study spurred by the demands of the aircraft and aerospace industries [1]. Due to their low density, high strength, and excellent corrosion resistance, titanium and its alloys are extensively used in aeronautical and chemical industries [2]. However, titanium and its alloys show poor resistance to wear and oxidation [3]. Laser cladding is a laser processing technique, and laser cladding ceramic coating or the ceramic particles reinforcement composite coating [4] is suitable for improving the surface performance of titanium alloy.

Titanium aluminides are attracting more and more attention recently due to their merits of low density, high specific strength, elastic modulus, wear resistance, oxidation resistance and better mechanical behavior with temperature [5]. TiB_2 ceramics have excellent physical and chemical properties such as high melting point, high hardness, good wear resistance and thermal and chemical stability [6]. Moreover, TiB_2 is also compatible with liquid iron aluminide at 1450 °C [7], Slaughter and Das [8] showed that Fe_3Al alloys containing TiB_2, fabricated by a rapid solidification rate process, exhibited better room temperature elongation and high tensile strength. Addition of Al_2O_3 to these metal borides can further improve their fracture toughness, flexural strength, and impact resistance, which renders the Al_2O_3-reinforced boride composites a promising candidate for a variety of the applications including cutting tools, wear-resistant parts and high-temperature structural materials [9].

In our research, it was found that laser cladding of the $Fe_3Al + TiB_2/Al_2O_3$ alloy powder on Ti–6Al–4V alloy can form the $Ti_3Al/Fe_3Al + TiB_2/Al_2O_3$ ceramic layer, which can significantly increase the micro-hardness of the Ti–6Al–4V alloy. Our present work is aimed at the investigation of the microstructure and phase structure of the $Ti_3Al/Fe_3Al + TiB_2/Al_2O_3$ ceramic layer.

2. Experimental

The materials used in this experiment were Ti–6Al–4V alloy and alloy powders of Fe_3Al (≥99.5% purity, 200 μm), TiB_2 (≥99.5% purity, 250 μm) and Al_2O_3 (≥98.5% purity, 250 μm) for laser cladding. The size of Ti–6Al–4V alloy was 10 mm × 10 mm × 10 mm. The thickness of pre-placed alloy powders layer was 0.6–0.8 mm. The parameters and the materials of the experiment are shown in Table 1.

Cross-flow CO_2 laser cladding equipment with a beam diameter of 4 mm, was employed to melt the surface of the samples. During the laser cladding process, the powders were dissolved into the melted pool, leading to the surface of samples, and the surface oxidation was prevented by inert gas (Ar) with the flowing rate of 25 L/min. After laser cladding, the samples were polished and etched in a hydrofluoric acid + nitric acid aqueous solution. The volume ratio of hydrofluoric acid, nitric acid and aqueous solution was 1:2:3.

The micro-hardness distributions of the coatings were measured by HV-1000 microsclerometer. Microscope analysis and QUANTA200 scanning electron microscope (SEM) were used to observe the microstructure characteristics of the coatings. DMAX/2500PCX X-ray diffraction (XRD) was used to determinate the phase constitutes of the coatings.

* Corresponding author. Tel.: +86 531 88395991; fax: +86 531 88395991.
E-mail address: czchen@sdu.edu.cn (C. Chen).

0925-8388/$ – see front matter © 2011 Elsevier B.V. All rights reserved.
doi:10.1016/j.jallcom.2011.01.199

Table 1
The parameters of laser cladding process in the experiment.

Number	Substrate materials	Powders composition/wt.%	Laser power/W	Scanning speed/mm s^{-1}	Spot diameter/mm
Sample 1	Ti–6Al–4V alloy	Fe_3Al–45TiB_2–20Al_2O_3	700–1300	2–7	4
Sample 2		Fe_3Al–45TiB_2			
Sample 3		Fe_3Al–35TiB_2			

3. Results and analysis

3.1. Microstructure

Fig. 1a and b shows the microstructure of the overview cross-section of the coatings of samples 1 and 2. As can be seen from Fig. 1a, after laser cladding, the coating of sample 1 was free of pores and cracks with a sound metallurgical combination to the Ti–6Al–4V alloy substrate, and the structure of the coating of sample 1 exhibited compact and homogeneous. However, the pores and un-melted TiB_2 block were present in the coating of sample 2, and there was not an obvious interface zone between the coating and Ti–6Al–4V alloy substrate.

In cladding process, the reaction between TiB_2 and Al_2O_3 consumed a portion of TiB_2 in coating of sample 1. Thus, it can be deduced that the dilution rate of Ti–6Al–4V alloy to coating of sample 1 was higher than that of sample 2. Therefore, after laser cladding, the freezing time of the molten pool of sample 2 was shorter than that of sample 1, which led the steam not have enough time to escape and the pores were formed in coating [10]. On the other hand, because of the short freezing time of molten pool, the TiB_2 powder in coating of sample 2 cannot melt completely and un-melted TiB_2 block was retained in coating of sample 2 (see Fig. 1b).

3.2. XRD analysis

The diffraction results were compared with the results published by the Joint Committee on Powder Diffraction Standards (JCPDS), and the measured values were close to the d values published by JCPDS. As was shown in Fig. 2, it was located that the coating surface of sample 3 consisted of Ti, α-Al, Fe_3Al, Ti_3Al, TiAl, Al_3Ti and TiB_2 phases (see Fig. 2). This phase constitute was beneficial to improve wear resistance of the Ti–6Al–4V alloy surface, and the reinforcement of the coating of sample 3 was mainly contributed to the action of the $Ti_3Al/Fe_3Al + TiB_2$ hard phases. In fact, in cladding process, a portion of the Fe_3Al phases in the coating of sample 3 can be dissolved due to the high temperature generated by the impingement of laser beam and powders, thus resulting to deliver Fe and Al particles in the molten pool of $Fe_3Al + 50$ wt.%TiB_2. Moreover, it should be also considered that the Al particles in the molten pool also came from the Ti–6Al–4V substrate. Thermodynamically, a portion of the Al particles had high affinity with Ti from the Ti–6Al–4V alloy substrate, thus the follow react between Al and Ti may take place leading to the formations of the Ti_3Al, TiAl and Al_3Ti phases.

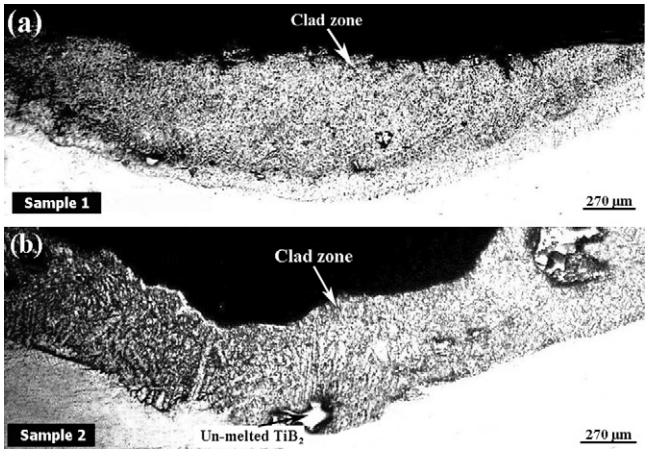

Fig. 1. Microstructure of the overview cross-section of (a) the coating of sample 1 and (b) the coating of sample 2.

As shown in Fig. 3, it can be seen that there were mainly Ti, α-Al, Fe_3Al, Ti_3Al, Al_2O_3 and TiB_2 phases in the coating surface of sample 1, and the reinforcement of the coating of sample 1 was mainly contributed to the action of the $Ti_3Al/Fe_3Al + TiB_2/Al_2O_3$ hard phases and the grain refinement. Moreover, the matrix of the coating mainly consisted of the Ti_3Al/Fe_3Al phases. It was also noted that the diffraction peak of TiB_2 of the coating of sample 1 was significantly weaker than that of the coating of sample 2. Nevertheless, its diffraction peak of Ti_3Al was stronger. It was reasonable to deduce that in laser cladding process, a large number of the Ti_3Al phases were produced in the coating of sample 1, in contrast amount of the TiB_2 phases vanished. It revealed that the chemical reactions between a part of the Al_2O_3 and TiB_2 phases took place as follows:

$$Al_2O_3 + 6TiB_2 \rightarrow 2Ti_3Al + 12B + 3/2O_2 \quad (1)$$

It was interesting to note that the feature of the phase constituents of the coating of sample 1 was absence of the TiAl and Al_3Ti phases, which had been found in the coatings of samples 2 and 3. As mentioned previously, a portion of TiB_2 in the coating had been lost due to the reaction of Eq. (1), thus resulting the increase of the dilution rate of Ti–6Al–4V alloy to the coating. Therefore, amount of the un-consumed TiB_2 in coating can obtain enough energy from the laser beam, and then dissolved to deliver Ti and B particles into molten pool. On the other hand, increase of the dilution rate caused more Ti and Al from the Ti–6Al–4V alloy substrate enter into the molten pool. Nevertheless, as known that the mass fraction of Ti was significantly greater than that of Al in Ti–6Al–4V alloy. Hence, it can be speculated that with the increase of dilution rate, a Ti-rich molten pool was obtained. Thus, Ti can further react with $TiAl_3$ or TiAl leading to the formation of Ti_3Al, and these reactions can be described as follows:

$$8Ti + TiAl_3 \rightarrow 3Ti_3Al \quad (2)$$

$$2Ti + TiAl \rightarrow Ti_3Al \quad (3)$$

Eqs. (2) and (3) indicated that a large number of the Ti_3Al phases were produced, which can greatly increase the micro-hardness and the wear resistance of the coating of sample 1.

3.3. Microstructure of the $Ti_3Al/Fe_3Al + TiB_2/Al_2O_3$ ceramic layer

Fig. 4a shows that the Al_2O_3 and TiB_2 precipitated phases were dispersed in the Ti_3Al/Fe_3Al matrix of the coating of sample 1. In freezing time, the molten pool generated during laser cladding undergoes a high cooling, so fine Al_2O_3 dendrite and TiB_2 precipitated. In fact, the TiB_2 precipitated phase was formed by the

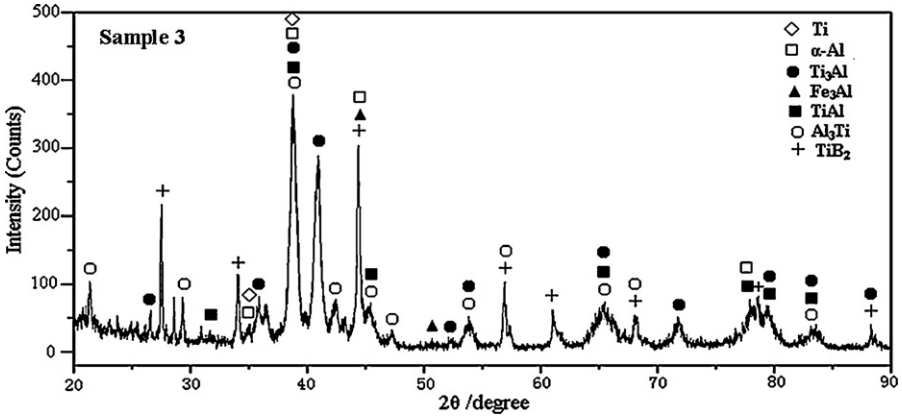

Fig. 2. X-ray diffraction diagram of the coating of sample 3.

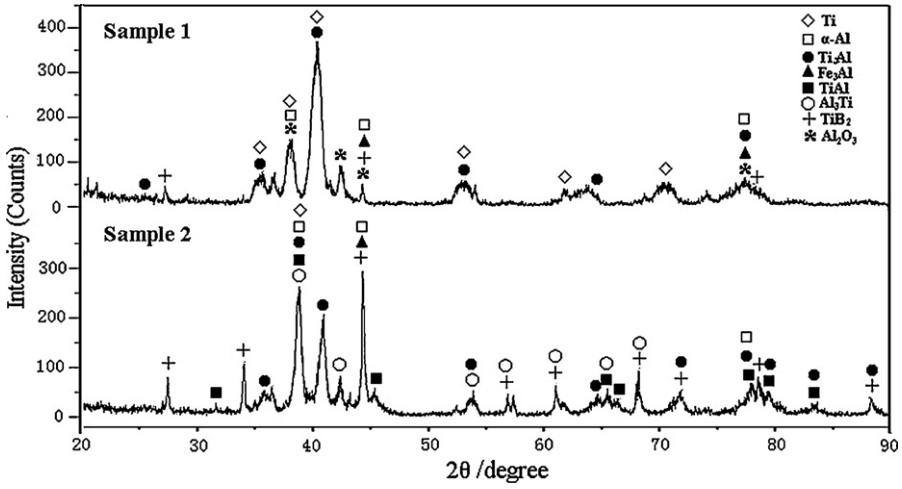

Fig. 3. X-ray diffraction diagram of the coatings of samples 1 and 2.

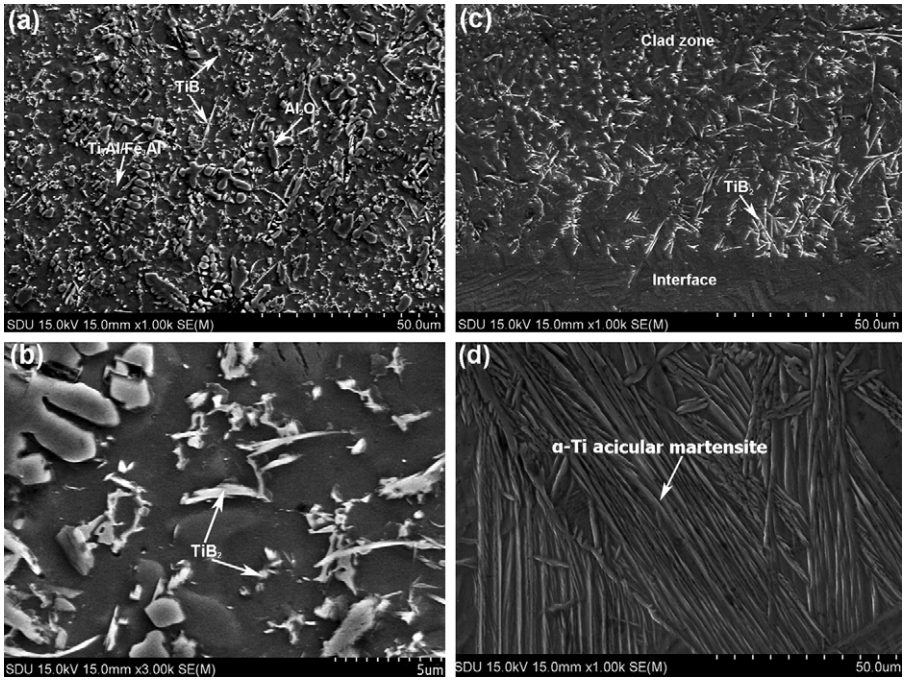

Fig. 4. The microstructure of the coating of sample 1, (a) near the surface, (b) TiB_2 precipitate phase, (c) interface zone, and (d) α-Ti acicular martensite.

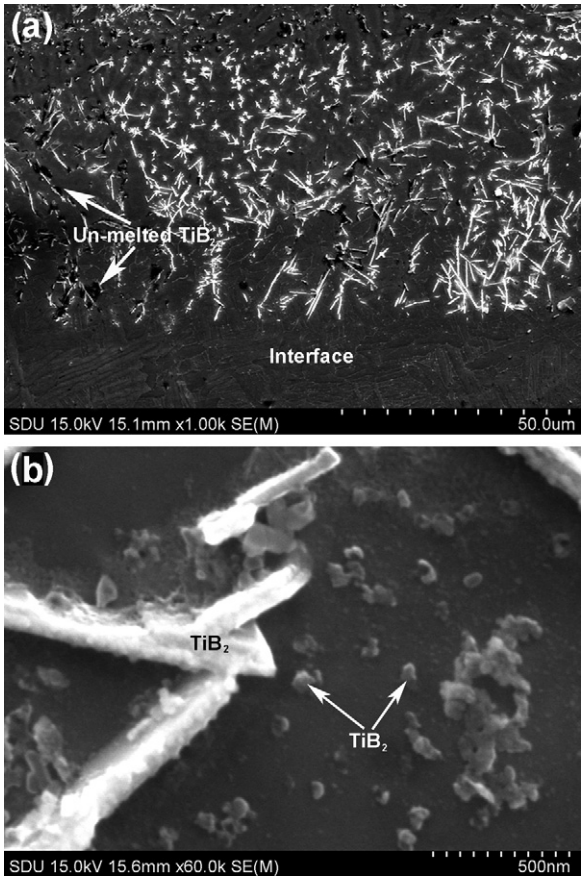

Fig. 5. SEM microstructure of the coating of sample 2 on Ti–6Al–4V alloy, (a) near the surface and (b) TiB_2.

melting–dissolution–reprecipitation mechanism, i.e. TiB_2 melted and dissolved into the molten liquid and during the cooling process TiB_2 nucleates and grew into the final reinforcement. In addition, most of the TiB_2 precipitated phases exhibited the fine acicular morphology due to the preferential growth of TiB_2 particle along the c axis ({0 0 0 1} direction) during the rapid cooling process of laser cladding [11] (see Fig. 4b). Moreover, combining the XRD result, it indicated that there was also α-Al in the matrix of the coating, nevertheless, due to the refinement of TiB_2, the grain boundary of α-Al cannot be exhibited clearly in SEM micrograph. The XRD result also indicated that the Al–Ti–B system was present in the coating of sample 1, which was composed of the TiB_2, Al_3Ti and Al phases, and the production of the Al–Ti–B system can further refine the structure of the coating [12–14]. Furthermore, the coating of sample 1 also demonstrated enough toughness, which can be proved by the fact that non cracking was shown in the coating [15].

Fig. 4c shows the microstructure of the region near the interface between the coating of sample 1 and the substrate. It demonstrated that TiB_2 showed distinctly different microstructures from the surface of coating to the interface. According to Eq. (1), in the cladding process, amount of boron was present in the molten pool, near the interface there also existed large amount of liquid titanium from the substrate in the molten pool, so the liquid titanium can react with boron leading to the formation of amount of TiB_2 in the interface zone. Moreover, during the freezing process when the cooling rate was greater than 200 °C/s, the martensite transformation completed without the diffusion, and the α-Ti acicular martensite was produced in the heat-affected zone [16] (see Fig. 4d).

Fig. 5 shows the microstructure of the coating of sample 2 on the Ti–6Al–4V alloy substrate. As mentioned previously, amount

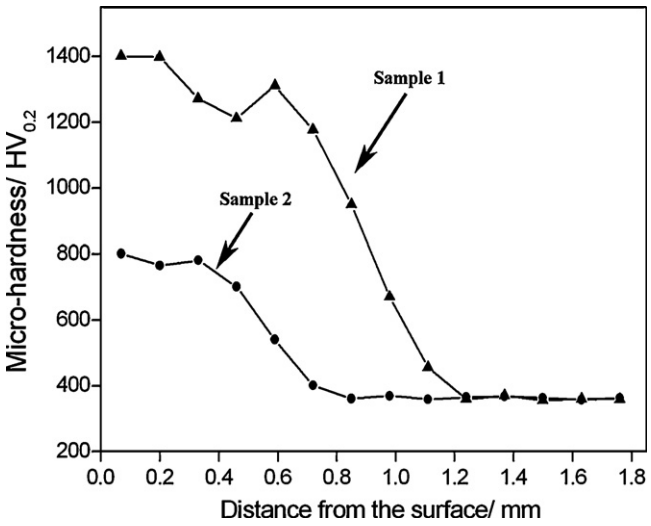

Fig. 6. The micro-hardness distributions of the coatings of samples 1 and 2.

of the un-melted TiB_2 blocks and TiB_2 precipitate phases retained in the coating of sample 2 after laser cladding (Fig. 5a). It was also noted the coating of sample 2 presented a microstructure essentially consisted of the fine TiB_2 reinforcing particles dispersed in the Ti_3Al/Fe_3Al matrix, and the TiB_2 particles exhibited faceted and blocky morphology, because of the rapid super-cooling rate, a part of the TiB_2 phases had very limited time to grow up, thus resulting in the fine size of a part of the TiB_2 particles in the Ti_3Al/Fe_3Al matrix (see Fig. 5b). On the other hand, it should be considered that the amount of the TiB_2 particles was engulfed during solidification within α-Al solid solution phases and appeared as small clusters [17].

3.4. The micro-hardness distribution

The micro-hardness distributions of the coatings of samples 1 and 2 as a function of depth from the top of coating to the Ti–6Al–4V alloy are shown in Fig. 6. It was found that with the increase of the distance from the surface to the Ti–6Al–4V substrate, the micro-hardness decreased.

Under the action of the $Ti_3Al/Fe_3Al + TiB_2/Al_2O_3$ phases and the grain refinement, the micro-hardness of the coating of sample 1 was in the range of 1200–1400 $HV_{0.2}$, which was 3–4 times higher than that of the Ti–6Al–4V alloy substrate. As mentioned before, especially the productions of Ti_3Al and the Al–Ti–B system significantly increased the micro-hardness and wear resistance of this coating.

In addition, the micro-hardness of the coating of sample 2 was in the range of 650–800 $HV_{0.2}$ due to the strength of the $Ti_3Al/Fe_3Al + TiB_2$ hard reinforcement phases. It was noted that the micro-hardness of the coating of sample 2 was lower than that of the $Fe_3Al + TiB_2/Al_2O_3$ coating due to lack of the action of Al_2O_3.

4. Conclusions

In this study, it was found that laser cladding of the $Fe_3Al + TiB_2/Al_2O_3$ pre-placed alloy powder on Ti–6Al–4V alloy can form the $Ti_3Al/Fe_3Al + TiB_2/Al_2O_3$ ceramic layer. In fact, in cladding process Al_2O_3 can react with TiB_2 in molten pool leading to the production of a large amount of B and Ti_3Al. This principle can be used to improve the microstructure performance and micro-hardness of the $Fe_3Al + TiB_2$ laser cladding layer on Ti–6Al–4V alloy. It was located that the $Fe_3Al + TiB_2/Al_2O_3$ coating surface mainly consisted of Ti, α-Al, Fe_3Al, Ti_3Al, Al_2O_3 and TiB_2 phases, and the present of the

Al–Ti–B system can refine the microstructure of the coatings. Due to action of the grain refinement and hard phases, the micro-hardness of the $Ti_3Al/Fe_3Al + TiB_2/Al_2O_3$ ceramic layer on Ti–6Al–4V alloy was significantly increased.

Acknowledgements

This work was supported by the Development Project of Science and Technology of Shandong Province (2006GG2204010) and Graduate Independent Innovation Foundation of Shandong University, GIIFSDU (31370070613156).

References

[1] S. Banumathy, P. Ghosal, A.K. Singh, J. Alloys Compd. 394 (2005) 181–185.
[2] E.C. Santos, M. Morita, M. Shiomi, K. Osakada, M. Takahashi, Surf. Coat. Technol. 201 (2006) 1635–1642.
[3] J. Dutta Majumdar, I. Manna, A. Kumar, P. Bhargava, A.K. Nath, J. Mater. Process. Technol. 209 (2009) 2237–2243.
[4] Q.W. Meng, L. Geng, D.R. Ni, Mater. Lett. 59 (2005) 2774–2777.
[5] S. PalDey, S.C. Deevi, T.L. Alford, Intermetallics 12 (2004) 985–991.
[6] W.H. Wang, Z.Y. Fu, H. Wang, R.Z. Yuan, J. Eur. Ceram. Soc. 22 (2002) 1045–1049.
[7] B.G. Park, S.H. Ko, Y.H. Park, J.H. Lee, Intermetallics 14 (2006) 660–665.
[8] E.R. Slaughter, S.K. Das, in: R. Mehrabian, B.H. Kear, M. Cohen (Eds.), Rapid Solidification Processing: Principles and Technologies, II, vol. 41, Charitor's Publishing Division, Baton Ronge, LA, 1999, pp. 39–49.
[9] M.L. Gu, C.Z. Huang, S.R. Xiao, H.L. Liu, Mater. Sci. Eng. A 486 (2008) 167–170.
[10] J.N. Li, C.Z. Chen, T. Squartini, Q.S. He, Appl. Surf. Sci. 257 (2010) 1550–1555.
[11] B.S. Du, A.N. Samant, S.R. Paital, N.B. Dahotre, Appl. Surf. Sci. 255 (2008) 3188–3194.
[12] C.X. Liu, J.H. Zhang, J.L. Sun, X.H. Zhang, Ceram. Int. 33 (2007) 1319–1324.
[13] G.S. Vinod Kumar, B.S. Murty, M. Chakraborty, J. Alloys Compd. 472 (2009) 112–120.
[14] P.T. Li, X.G. Ma, Y.G. Li, J.F. Nie, X.F. Liu, J. Alloys Compd. 503 (2010) 286–290.
[15] B.S. Du, Z.D. Zou, X.H. Wang, S.Y. Qu, Appl. Surf. Sci. 254 (2008) 6489–6494.
[16] J.N. Li, C.Z. Chen, L. Zong, Int. J. Refract. Met. Hard Mater. 29 (2011) 49–53.
[17] P.L. Schaffer, D.N. Miller, A.K. Dahle, Scripta Mater. 57 (2007) 1129–1132.